Challenge in Cu-rich $CuInSe_2$ thin film solar cells: Defect caused by etching

Hossam Elanzeery,[1,*] Michele Melchiorre,[1] Mohit Sood,[1] Finn Babbe,[1] Florian Werner,[1]
Guy Brammertz,[2,3] and Susanne Siebentritt[1]
[1]Laboratory for Photovoltaics, Physics and Materials Science Research Unit, University of Luxembourg, Belvaux L-4422, Luxembourg
[2]Imec Division IMOMEC, Partner in Solliance, Wetenschapspark 1, 3590 Diepenbeek, Belgium
[3]Institute for Material Research (IMO), Hasselt University, Partner in Solliance, Wetenschapspark 1, 3590 Diepenbeek, Belgium

(Received 21 December 2018; published 16 May 2019)

Thin-film solar cells consist of several layers. The interfaces between these layers can provide critical recombination paths and consequently play a vital role in the efficiency of the solar cell. One of the main challenges for polycrystalline semiconductor absorber materials is the absorber-buffer interface. The Cu(In, Ga)Se_2 system is particularly interesting in this context, since Cu-rich absorbers are dominated by recombination at the interface, while Cu-poor ones are not. This paper unveils the root cause of the challenge in the interface of Cu-rich solar cells in terms of a Se-related defect with an activation energy of 200 ± 20 meV. This defect causes interface recombination and is responsible for the deficiency of open-circuit voltage in Cu-rich cells. Moreover, this paper demonstrates that the origin of this defect is due to the etching step necessary to remove secondary phases. Postdeposition surface treatments or modified buffer layers are shown to passivate this defect, to reduce interface recombination, and to increase the efficiency.

DOI: 10.1103/PhysRevMaterials.3.055403

I. INTRODUCTION

Photovoltaics represent one of the promising technologies that are able to provide a renewable source of energy at very low costs with current production of almost 2% of global electricity [1]. Thin-film photovoltaic cells are considered milestones towards achieving high efficient solar cells with lower costs related to their low material and energy consumption, shorter energy payback time, and a wide range of possible applications and opportunities [2]. Chalcopyrite copper indium gallium diselenide (CIGS) represents one of the most promising absorbers for thin-film solar cells [3] characterized by their high efficiencies reaching 23.35% on a laboratory scale [4,5] and 15.0% for its ternary compound $CuInSe_2$ (CIS) [6]. CIS and CIGS grown under Cu excess, referred to as Cu-rich CI(G)S with [Cu]/[III] ratio > 1 and global ratio including secondary Cu selenides, present generally the better semiconductor properties compared to Cu-poor material: larger grains, higher mobility, lower defect densities, better transport properties [7–10], and better collection efficiency [11]. All record solar cells, however, have been prepared from Cu-poor absorbers, because of their higher open-circuit voltage and thus efficiency. The low open-circuit voltage of Cu-rich chalcopyrite solar cells is linked to interface recombination [12]. Nevertheless, it is important to note that a transitory Cu-rich phase during growth has played a significant role in controlling the stress release and the optimization of the absorber quality during growth [3,13]. State-of-the-art CIGS record cells are based on a three-stage absorber fabrication process, which involves Cu-poor and Cu-rich phases [14]. Thus, it is important for the thin-film community to understand the reason behind the lower efficiencies in Cu-rich thin-film solar cells. The lower efficiency in Cu-rich cells compared to Cu-poor ones is due to a strong decrease in the open-circuit voltage (V_{OC}). The root cause behind this V_{OC} deficit is recombination at the absorber-buffer interface [12,15,16]. Interface challenges play a vital role in defining the quality and the efficiency of all solar cells. The interface challenges for polycrystalline semiconductor absorbers like CIGS become even more complex. For Cu-rich thin-film solar cells, the root cause of such interface challenges was not clear but has traditionally been attributed to the absence at the surface of the Cu-rich absorbers of an ordered defect compound (ODC) with a higher band gap [12,17]. However, high-resolution methods like transmission electron microscopy or atom probe tomography generally fail to detect the composition of an ODC at the surface of Cu-poor absorbers [7]. Therefore, we have proposed in the past tunnel recombination near the interface due to the high absorber doping of Cu-rich material [16,18]. However, it is difficult to explain the observed dramatic decrease of V_{OC} in Cu-rich solar cells based on a steep band bending alone. Several approaches have been developed to combine Cu-rich absorbers with a Cu-poor surface by implementing different surface treatments [11,16,19–21] that were reported to increase the V_{OC} of Cu-rich cells through the reduction of interface recombination. Recently, it was found that the V_{OC} gap between Cu-rich and Cu-poor cells is related to the bulk recombination and not only to the interface: the quasi-Fermi-level splitting (qFLs), that represents the highest V_{OC} an absorber can achieve, is lower for Cu-rich Cu(In, Ga)Se_2 than for Cu-poor Cu(In, Ga)Se_2, even before the interface with the buffer is formed [22,23]. The same study demonstrated a considerably larger difference between qFLs and V_{OC} in Cu-rich solar cells, indicating that interface recombination

*hossam.elanzeery@gmail.com

 ©2019 American Physical Society

poses an additional loss mechanism in Cu-rich Cu(In, Ga)Se_2. This was confirmed by the investigation of the diode factor in Cu-rich and Cu-poor absorbers and solar cells [24]. In summary: Cu-rich Cu(In, Ga)Se_2 solar cells suffer from interface recombination, but it is not clear why the buffer-absorber interface is different from the one with Cu-poor absorbers.

According to the phase diagram [25], Cu-rich absorbers are characterized by a stoichiometric chalcopyrite phase with additional copper selenide (Cu_2Se) secondary phases. Etching these conductive secondary phases is mandatory for the electrical performance of such cells [26,27]. This paper unveils one of the main causes for the dominating interface recombination in Cu-rich solar cells by presenting that this essential etching step is responsible for the formation of defects near the surface acting as recombination centers and deteriorating the performance of such cells. Moreover, this paper highlights the characteristics of such defect and provides means of passivating this defect, restoring part of the lost V_{OC} and leading to an increase in the efficiency of Cu-rich solar cells.

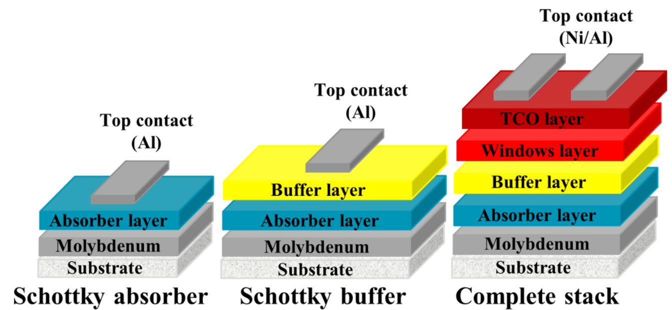

FIG. 1. Three different absorber structures: "Schottky absorber" is the bare absorber covered with an aluminum (Al) Schottky contact; "Schottky buffer" is the absorber covered with a CdS buffer layer, then covered with an aluminum Schottky contact; and "complete stack" is the fully processed solar cell.

II. RESULTS AND DISCUSSIONS

A. Identification of defects in Cu-rich CIS thin-film solar cells

To understand the reason behind the V_{OC} deficit, responsible for the lower efficiency in Cu-rich cells compared to Cu-poor ones, we performed different characterization techniques to identify and analyze defects in Cu-rich CIS that is the ternary end composition of state-of-the-art CIGS thin-film solar cells. We performed capacitance measurements as a function of frequency and temperature (admittance measurements) in order to identify the main capacitance steps in Cu-rich CIS. These capacitance steps could be either defects or barriers as explained in the experimental section. In this section, we present the main capacitance step in Cu-rich CIS with an activation energy of 200 ± 20 meV, comparing it to Cu-poor values and showing how we identified this 200 ± 20 meV step as a defect and not a barrier.

Admittance measurements (ADM) were performed for Cu-rich and Cu-poor CIS solar cells. The capacitance values are plotted as a function of frequency and temperature. The main capacitance step (where a barrier or a defect is likely to respond) is identified by two short dashed lines in all admittance spectra presented in this paper (see Fig. 2 for example). The inflection points of these steps are determined from the maxima in the derivative with respect to the log of the frequency as explained in the experimental section below. The values are plotted in an Arrhenius plot. The activation energy of the main capacitance step is then calculated from the slope of the linear fit of this Arrhenius plot [28].

The activation energy of the main capacitance step revealed from ADM measurements indicates an activation energy of 200 ± 20 meV for the step in Cu-rich cells, while an activation energy of 130 ± 10 meV is deduced in the case of Cu-poor CIS cells [29]. It is important to note that this 200 ± 20 meV capacitance step is present in all our Cu-rich CIS cells whether or not we change the Cu/In ratio or Se flux as reported earlier [30]. The nature of this 200 ± 20 meV step is not *a priori* clear, i.e., whether it is a barrier or a defect and whether it is at the interface or the bulk of the absorber. To unveil the nature of this step, several experiments were performed.

Three Cu-rich absorber runs were fabricated with three different Se fluxes (low, medium, and high). The pressure of the low Se flux is in the range of 4×10^{-6} mbar, medium Se flux is in the range of 1×10^{-5} mbar, and high Se flux is in the range of 4×10^{-5} mbar. Our standard Cu-rich CIS absorber deposition process is performed using the lowest possible Se flux (pressure of 4×10^{-6}) mbaras lower Se flux has been reported to be more beneficial for our Cu-rich CIS cells [18] and Se fluxes with pressure lower than 4×10^{-6} mbar are not sufficient to form the required CIS phase.

Each absorber fabrication run contains four similar absorbers. One sample was kept for reference and the other three samples were etched using strong potassium cyanide (KCN) etching that is necessary to remove conductive copper selenide secondary phases as explained in the experimental section. The three samples are then completed in three different levels referred to in the text as "Schottky absorber," "Schottky buffer," and "complete stack" as presented in Fig. 1 and explained in the experimental section. Aluminum (Al) is deposited on top of the absorber in the case of the Schottky absorber and on top of the absorber-buffer surface in the case of the Schottky buffer to form a Schottky contact [31,32]. ADM measurements were then performed for the three samples of each of the three absorbers with different Se fluxes with a total of nine samples. The activation energy of the main capacitance step was then deduced from the slope of the Arrhenius plot for all nine samples. The admittance spectra and Arrhenius plots of the three different samples of one of the absorber runs (absorber with medium Se flux) are presented in Figs. 2(a)–2(d). The temperature scale of the ADM measurements in Figs. 2(a)–2(c) is presented on the left side of Fig. 2.

Figure 2(a) represents the ADM spectrum for the Cu-rich CIS absorber with Schottky contact. Three main capacitance steps could be revealed from Fig. 2(a) as indicated by the short-dashed lines. A high-temperature step (represented as step 1) has an activation energy of 280 meV, a medium-temperature step (represented as step 2) has an activation energy of 208 meV, and a low-temperature step (represented as step 3) has an activation energy of 60 meV. After adding

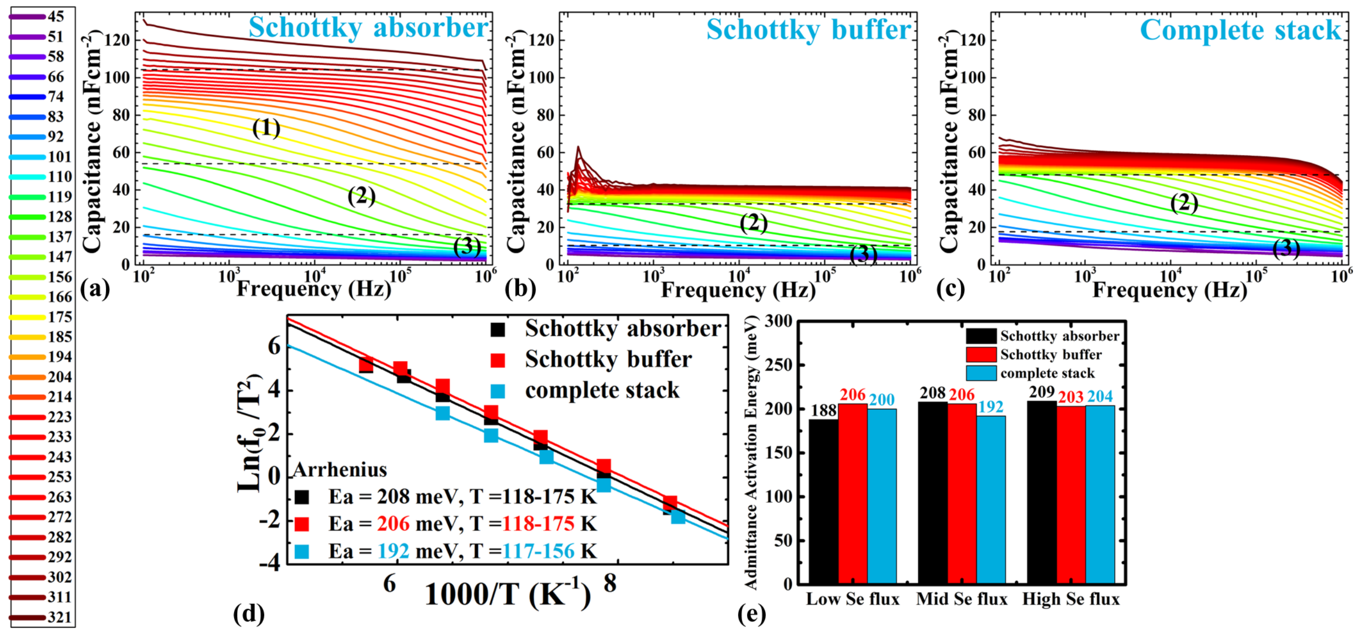

FIG. 2. Admittance measurements for (a) Schottky absorber, (b) Schottky buffer, and (c) complete stack of a Cu-rich CIS solar cell grown with a medium Se flux, measured between 320 and 50 K as indicated by the temperature scale on the left side. (d) The Arrhenius plot for Schottky absorber, Schottky buffer, and complete stack Cu-rich CIS (a–c) indicating the activation energy of the main capacitance step with values around 200 ± 20 meV for the three samples at the same temperature range (117–175 K). (e) Activation energies deduced from admittance measurements for Schottky absorber, Schottky buffer, and complete stack for three Cu-rich CIS grown under different Se flux conditions (low, medium, and high Se fluxes). The main capacitance step of all samples indicates activation energy of 200 ± 20 meV.

a CdS buffer layer in Fig. 2(b), the high-temperature step disappears, leaving only steps 2 and 3 of the medium and low temperatures. The high-temperature step (with an activation energy of 280 meV) could be explained as a defect that was caused by the Al contact or passivated by the CdS buffer layer and is not the main focus of this paper. Further processing of the sample in Fig. 2(c) reveals that the medium- and low-temperature steps remain the same with no additional changes. The low-temperature step can be attributed to freeze-out and could represent the activation energy of the doping defect [10]. Therefore, the main capacitance step for the three samples is the one at intermediate temperatures (step 2) and will be the main focus of this paper. The activation energy of the main capacitance step (medium temperature) for the three samples deduced from the Arrhenius plot in Fig. 2(d) indicates an activation energy of 200 ± 20 meV in the same temperature range (117–175 K). The same trend was observed for the other two absorber runs with different Se fluxes and the activation energies of the main capacitance step for all nine samples are presented in Fig. 2(e). Figure 2(e) shows that the activation energy of the main capacitance step for all nine samples is the same with a value of 200 ± 20 meV and in the same temperature range regardless of the Se flux used. This capacitance step is present on absorbers with only Schottky contacts and no buffer or window layers, indicating that this capacitance step is a property of the absorber. Based on that, this step could be either a bulk defect or a barrier at the absorber back interface (Mo-CIS interface).

If this capacitance step was due to a barrier, then the activation energy of the thermally activated series resistance or the forward bias current should indicate values close to that extracted from admittance measurements (200 ± 20 meV), otherwise this step would be a defect as explained in the experimental section.

To quantify that, both the series resistance and forward bias current as a function of temperature were deduced from the current-voltage (IV) measurements as a function of temperature (IVT) performed under dark conditions. The series resistance was extracted from the slope of the IV curves at far forward bias (1.2 V) as a function of temperature. At far enough forward bias, the current is limited by either the transport of holes over the back interface barrier between the absorber and the back contact or the transport of electrons at the front interface barrier between the absorber and buffer layers [33], and the series resistance (R_S) is then thermally activated [34]. The activation energies of both the thermally activated series resistance and forward bias current [35] in Cu-rich CIS solar cells were deduced from the slope of their corresponding Arrhenius plots (Fig. S1 in Supplemental Material [36]), indicating values in the range of 100 ± 10 and 55 ± 5 meV for the thermally activated series resistance and forward bias current, respectively. These values are much lower than that of the main capacitance step (200 ± 20 meV) in the same temperature range (117–175 K). This means that the main capacitance step in Cu-rich CIS thin-film solar cells is indeed a defect in the absorber and not a barrier with an activation energy of 200 ± 20 meV.

B. Means of passivating defects in Cu-rich CIS

As explained above, Cu-rich CIS thin-film solar cells suffer from a defect with an activation energy around 200 ± 20 meV.

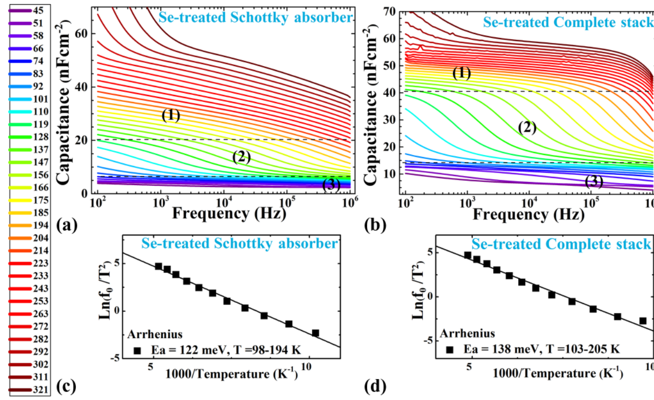

FIG. 3. Admittance measurements for (a) Schottky absorber and (b) complete stack of Se-PDT Cu-rich CIS solar cells for temperatures between 320 and 50 K as indicated by the temperature scale on the left. The Arrhenius plot indicates the activation energy of the main capacitance step for (c) Schottky absorber and (d) complete stack Se-PDT Cu-rich CIS solar cells.

This defect was previously passivated using different types of postdeposition treatments (PDTs) such as *ex situ* potassium fluoride (KF) [11], *in situ* KF [20], and In-Se [37] PDTs with a corresponding increase in the V_{OC} after such treatments. After identifying and understanding the nature of this defect as an absorber-related defect, the question arises if we can passivate this defect by modifying the absorber surface using simpler postdeposition treatments than the reported ones or by simply using a modified buffer. In the following two subsections, we will provide means of passivating this 200 ± 20 meV defect using Se-only PDT (Sec. II B 1) and using modified buffer layers (Sec. II B 2).

1. Passivating defects using Se postdeposition treatment

Se is the common player in all PDTs (In-Se [19,37], *ex situ* KF [11], and *in situ* KF [20]) passivating the 200 ± 20 meV defect. It is interesting to discover if a Se-only PDT would also passivate this defect leading to similar improvements to the ones reported in those PDTs or the passivation of the defect was related to In and KF parts of those PDTs.

Four Cu-rich CIS absorbers of the same batch were etched using strong KCN to remove conductive secondary phases as explained earlier. One absorber was used as a reference, ADM measurements were performed on it, and the presence of the 200 ± 20 meV defect was confirmed. Then, the remaining three absorbers were all treated with a Se-only PDT, explained in the experimental section and then completed in the same way as explained earlier as the Schottky absorber, Schottky buffer, and complete stack (Fig. 1). ADM measurements were performed for the three samples and the three of them indicated an activation energy of 130 ± 10 meV for the main capacitance step as reported [29] and presented in Fig. 3. Figure 3(a) represents the admittance spectra for the Schottky absorber treated with Se-only PDT showing three capacitance steps as explained earlier. The high-temperature step (step 1) could not be resolved within the measurement range and the low-temperature step (step 3) is related to freezeout with an activation energy of 60 meV. The main capacitance step is again the medium-temperature one (step 2) with an activation energy of 122 meV as deduced from the slope of the Arrhenius plot in Fig. 3(c). The activation energy of the main capacitance step (130 ± 10 meV) in Schottky absorbers treated with Se-only PDT lies much below that of the untreated Schottky absorbers (200 ± 20 meV), indicating the passivation of this 200 ± 20 meV defect. Moreover, the success of the Se-only PDT in passivating this defect with no buffer layers proves that this defect is related to the absorber and is a Se-related defect. The admittance spectrum for the complete stack of the Se-treated absorber is presented in Fig. 3(b) with the main capacitance step indicated by the two short-dashed lines. The temperature scale for the admittance spectra is presented on the left side of Fig. 3. The activation energy of the Se-treated complete stack sample is extracted from the Arrhenius plot in Fig. 3(d) showing a value of 138 meV, which lies in the range of 130 ± 10 meV. The presented activation energies in Figs. 3(c) and 3(d) are much less than that of the untreated samples (200 ± 20 meV), confirming that the Se-only PDT is able to passivate this (200 ± 20 meV) defect, indicating that this defect is Se related.

The disappearance of the 200 ± 20 meV defect using the Se-only PDT is accompanied by an increase in the V_{OC} by around 30 mV, increase in the fill factor (FF) by 10% absolute, and a corresponding increase in the efficiency by 2% absolute as presented in Table I. The increase in the V_{OC} as a function of passivating the 200 ± 20 meV defect has been observed after treating Cu-rich CIS with *ex situ* KF [11], *in situ* KF [20], and In-Se [19,37] PDTs.

2. Passivating defects using modified buffer layers

Passivating the 200 ± 20 meV defect can also be achieved by modifying the buffer layer. From Sec. II B 1, it was concluded that the 200 ± 20 meV defect is a Se-related defect. It was then interesting to discover if using a buffer layer with higher sulphur concentrations would also lead to the passivation of this defect. First, we used a modified CdS buffer layer deposited at Swiss Federal Laboratories for Materials Science and Technology (EMPA) (characterized by its relatively high thiourea concentration and longer durations [38]) as well as a standard Zn(O,S) buffer layer developed in-house

TABLE I. *IV* parameters extracted from *IV* measurements under standard test conditions for the average of six solar cells for each of the Cu-rich and Se-treated Cu-rich CIS solar cells. Values in brackets represent the *IV* parameters of the best solar cell.

Sample	Efficiency (%)	FF (%)	V_{OC} (mV)	J_{SC} (mA/cm^2)	R_s Ω cm^2	R_{sh} Ω cm^2
Cu-rich CIS	7.0 (7.7)	46.8 (50.3)	355 (357)	42.1 (44.3)	0.5 (0.4)	124 (198)
Se-treated Cu-rich CIS	9.2 (9.4)	59.2 (60.6)	382 (385)	40.7 (42.3)	0.4 (0.3)	794 (1153)

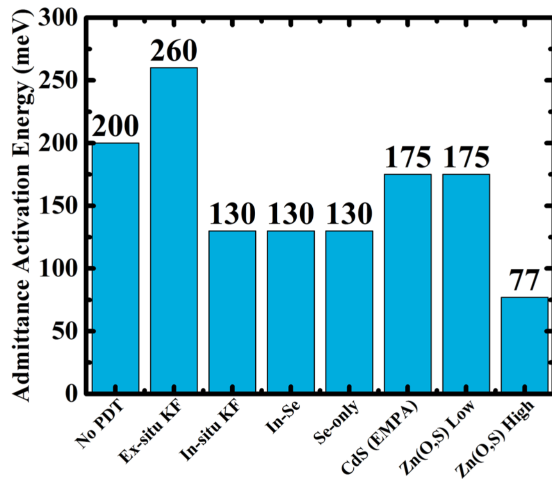

FIG. 4. Summary of the activation energies deduced from admittance measurements for different PDTs and buffer layers.

with slightly higher thiourea concentrations compared to our standard baseline CdS buffer layer. ADM measurements were performed on Cu-rich CIS etched absorbers with these two buffer layers and aluminum front contacts forming a Schottky junction. The activation energy for the main capacitance step in both cases showed values of 175 ± 5 meV, slightly lower than the values of 200 ± 20 meV as presented in Fig. 4, indicating the passivation of this defect. Motivated by these results, a Zn(O,S) buffer layer with much higher thiourea concentrations compared to our standard Zn(O,S) one (eight times higher thiourea concentration) was deposited on a similar Cu-rich CIS etched absorber. The activation energy deduced from the ADM measurements of this sample with much higher thiourea concentrations showed values of 77 ± 5 meV, significantly lower than the values of 175 ± 5 meV with standard lower thiourea concentrations as presented in Fig. 4. This means that modified buffer layers with high enough thiourea concentrations (high sulphur contents) are able to passivate the 200 ± 20 meV Se-related defect. Not only that, but interestingly the V_{OC} increased by more than 70 mV for the Cu-rich CIS with Zn(O,S) of high thiourea concentration compared to the same Cu-rich CIS absorber but with standard CdS buffer layer as a consequence of passivating the 200 ± 20 meV defect. The improvement in the V_{OC} (ΔV_{OC}) of Cu-rich CIS cells as a result of passivating the 200 ± 20 meV defect using PDTs with high enough Se and modified buffer layers with high enough S, compared to Cu-rich CIS cells with standard CdS buffer layer, is summarized in Table II. No device was fabricated from the Cu-rich CIS absorber with standard Zn(O,S) buffer layer (Zn(O,S) Low thiourea).

A summary of the activation energies deduced from ADM measurements for different PDTs and buffer layers is presented in Fig. 4. It can be concluded from Fig. 4 that the 200 ± 20 meV defect can be passivated by *ex situ* KF, *in situ* KF, In-Se and Se-only PDTs, as well as CdS and Zn(O,S) buffer layers with high enough chalcogen concentrations. The high activation energy presented for the *ex situ* KF PDT (260 ± 20 meV) has been related to a barrier and not to the 200 ± 20 meV defect. The characteristics of passivating the 200 ± 20 meV defect (explained in Sec. II C) were observed after performing the *ex situ* KF PDT as presented in Fig. S2 in Supplemental Material [36].

TABLE II. A summary for the improvement in the values of the open-circuit voltage (ΔV_{OC}) of Cu-rich CIS solar cells after passivating the 200 ± 20 meV defect using PDTs and buffer layers with high enough chalcogen, compared to Cu-rich CIS solar cells with our standard CdS buffer layer.

Type of treatment	Improvement in V_{OC} (ΔV_{OC})
Ex situ KF (PDT)	35 mV [11]
In situ KF (PDT)	60 mV [20]
In-Se (PDT)	100 mV [19]
Se only (PDT)	30 mV
EMPA CDs (buffer)	35 mV
Zn(O,S) High *s* (buffer)	70 mV

C. Characteristics of defects in Cu-rich CIS

This section highlights the characteristics of the 200 ± 20 meV defect, its negative effects on the electrical performance of Cu-rich CIS thin-film solar cells, as well as the positive impacts taking place after passivating this defect.

From the discussions above, it can be concluded that the first characteristic of this 200 ± 20 meV defect is that it is responsible for decreasing the V_{OC} and passivating such defect is always associated with an improvement in the V_{OC} values.

The second characteristic is related to the ADM measurements. Normally, for Cu-rich CIS cells, the admittance derivatives (explained in Sec. II A) from which the inflection points of the main capacitance step (200 ± 20 meV) are extracted are characterized by broad peaks, much broader than those of Cu-poor solar cells (130 ± 10 meV) that are narrow as depicted in Figs. 5(a) and 5(b). After passivating this 200 ± 20 meV defect, the admittance peaks of the corresponding main capacitance step become narrow again, like the Cu-poor case. The admittance peaks for the Se-PDT Cu-rich CIS of the same absorber are presented in Fig. 5(c) (narrow peaks) as an example of the admittance peak behavior after the passivation of the 200 ± 20 meV defect from the same absorber.

Moreover, it is interesting to note that the main capacitance step for Cu-rich CIS after Se-only [Fig. 3(c)], In-Se [37], and *in situ* KF [20] PDTs with an activation energy of 130 ± 10 meV occurs in the same temperature range as the main capacitance step before PDTs (200 ± 20 meV step). This means that the broad behavior of Cu-rich admittance peaks [Fig. 5(a)] reveals the presence of two defects lying in the same temperature range and overlapping each other, making their corresponding peaks broad. These two defects are the 200 ± 20 and 130 ± 10 meV defects. Only the one with higher activation energy (200 ± 20 meV) appears in the admittance spectra for untreated Cu-rich CIS while the other is hidden below, but broadens the peak in the derivative curves. After performing a PDT, the 200 ± 20 meV defect is removed and then the other defect with lower activation energy (130 ± 10 meV) appears with a narrow peak [Fig. 5(c)]. This hypothesis is also confirmed by the photoluminescence (PL) measurements presented in Fig. 5(d). In Fig. 5(d), a PL peak at 0.9 eV is present in Cu-rich CIS spectra before and

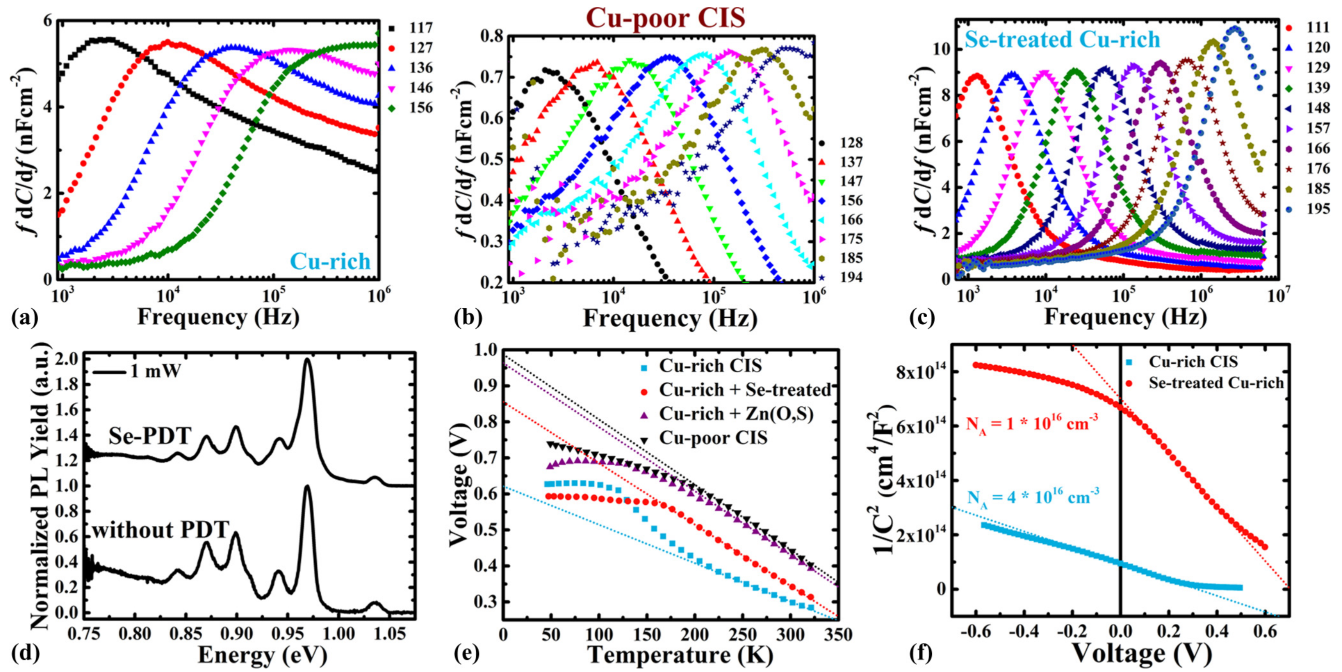

FIG. 5. Capacitance derivatives of the main admittance step in (a) Cu-rich, (b) Cu-poor, and (c) Cu-rich cases with Se PDT. The peaks of the capacitance derivatives are broad in the Cu-rich case and narrow in the case of Cu rich treated with Se PDT and in the Cu-poor case. The numbers on the right side of each plot indicate the temperature in degrees Kelvin for each of the corresponding presented curves. (d) Normalized PL spectra for Cu-rich and Se-treated Cu-rich cases at a power intensity of 1 mW. The 0.9 eV defect peak is present before and after the Se PDT. (e) Temperature dependence of the open-circuit voltage for Cu-poor (black), Cu-rich (blue), Se-treated Cu-rich (red), and Cu-rich with Zn(O,S) of high thiourea concentration (purple) CIS solar cells. A linear fit at high temperatures (short dotted line) is used to extract the activation energy of the reverse saturation current at 0 K. (f) Capacitance-voltage (CV) measurements of untreated Cu-rich CIS (blue) and Se-treated Cu-rich CIS (red) solar cells. The apparent doping is extracted from the inverse slope of a linear fit at small forward bias as indicated by the short-dotted line.

after the Se-only PDT measured at power intensity of 1 mW. This 0.9 eV peak has been proven to be a defect and reported to be likely the third acceptor defect (A3 defect), in the donor-acceptor pair transition DA3, with an activation energy of $130 \pm 10\,\text{meV}$ potentially related to indium vacancy [39]. The defect energy determined from this 0.9 eV PL peak is in excellent agreement with the admittance activation energy ($130 \pm 10\,\text{meV}$) and proving our hypothesis that the $130 \pm 10\,\text{meV}$ admittance step is a defect present in Cu-rich CIS solar cells before and after Se-only, In-Se, and *in situ* KF PDTs.

The third characteristic for the $200 \pm 20\,\text{meV}$ defect is related to the IVT measurements. The activation energy of the dominant recombination path in thin-film solar cells is deduced by extrapolating the temperature-dependent V_{OC} to 0 K. If the activation energy is close to the band gap, then the dominant recombination path is in the bulk of the absorber [40]. Otherwise, if the activation energy at 0 K is less than the band gap, then the dominant recombination path is at the interface of the absorber [41]. In Cu-rich thin-film solar cells, the extrapolated activation energy of the dominant recombination path at 0 K shows values lower than the band gap as presented in Fig. 5(e) (blue curve). This indicates that the dominant recombination path is at the interface of the Cu-rich absorbers as reported [11]. In Cu-poor CIS, the corresponding extrapolated activation energy is close to the band gap, indicating that the dominant recombination path is in the bulk of the absorber [11] as presented in Fig. 5(e) (black curve). With a Se-PDT (red curve) or Zn(O,S) buffer layer with high thiourea concentrations (purple curve), the extrapolated activation energy at 0 K improved to values closer to the band gap as presented in Fig. 5(e), indicating less influence of the interface recombination in Cu-rich CIS cells. Therefore, it can be concluded that the passivation of the $200 \pm 20\,\text{meV}$ values is always accompanied by an improvement in the activation energy of the dominant recombination path as presented for Se-PDT and Zn(O,S) buffer layer with high thiourea concentrations [Fig. 5(e)] and previously reported with the In-Se [19,37], *ex situ* [11], and *in situ* [20] KF PDTs.

The fourth characteristic is related to the slope of the V_{OC} curve as a function of temperature in Fig. 5(e). In Fig. 5(e), the V_{OC} (T) curve for Cu-rich CIS cells (blue curve) shows two different slopes and not one slope as normally observed for the Cu-poor case (black curve) before the V_{OC} values saturate at low temperatures. With the Se PDT (red curve) and Zn(O,S) with high thiourea concentrations (purple curve), one of the two slopes that used to be present for Cu-rich CIS cells disappeared as a result of passivating the $200 \pm 20\,\text{meV}$ defect, leaving only one slope similar to the Cu-poor case (black curve) as illustrated in Fig. 5(e). The second slope in Cu-rich CIS cells coincides with a strong temperature dependence of the photocurrent at V_{OC}, which makes the model for the activation energy invalid. The

relation between the disappearance of the 200 ± 20 meV defect and disappearance of the second slope in the V_{OC} (T) was also reported with *ex situ* [11] and *in situ* [20] KF PDTs.

The fifth characteristic is linked to the nature of this 200 ± 20 meV defect being an acceptor or donor. Capacitance-voltage (CV) measurements were performed for Cu-rich CIS before and after a Se PDT [Fig. 5(f)]. The inverse slope of the capacitance curves fitted at small forward bias in the Mott-Schottky plot presented in Fig. 5(f) was used to extract the apparent doping as explained in the experimental section. In Fig. 5(f), Cu-rich CIS has an apparent doping of 4×10^{16} cm^{-3} (blue curve) that decreased to 1×10^{16} cm^{-3} (red curve) after performing the Se PDT and passivating the 200 ± 20 meV defect. Similar trends of decreasing the apparent doping were observed after the passivation of the 200 ± 20 meV defect by all other different PDTs such as the *in situ* KF [20] and on all three different absorber structures (Schottky absorber, Schottky buffer, and complete stack). Based on that, it can be concluded that this defect is an acceptor defect.

We clearly show that the signature of the 200 ± 20 meV defect disappears from the admittance spectra. However, it was shown in the past that a defect signature can vanish without the defect disappearing by a distortion of the band bending: defects seen in a metastable state of the device disappeared in the relaxed state of the device [42,43]. To check if this could be the case, we placed two devices where we believe the 200 ± 20 meV defect has disappeared (one with high thiourea concentrations and the other with the Se PDT) into various metastable states and compared admittance and *IVT* results with the relaxed state. No metastable behavior could be observed (Figs. S3–S5 in Supplemental Material [36]). Thus, we can conclude that the signature disappears after the PDT because the 200 ± 20 meV defect has in fact been removed from the absorber.

D. Origin of defects in Cu-rich CIS

In the previous sections, we identified a defect that is only present in Cu-rich CIS thin-film solar cells, not in Cu-poor ones. We showed that removing this defect by various PDTs improves the open-circuit voltage. In this section, we will dig more into the possible root causes responsible for the formation of such defects.

Cu-rich CIS by definition is a stoichiometric CIS phase in addition to copper selenide secondary phases according to its phase diagram [25]. Therefore, the origin behind the formation of the Se-related 200 ± 20 meV defect should be related to either a defect present in the stoichiometric CIS phase or the additional copper selenide secondary phases and their etching process.

To differentiate between these two potential causes, a stoichiometric CIS absorber was fabricated. This absorber has a Cu/In ratio of 1.0, as measured by energy dispersive x-ray spectroscopy (EDX), before and after KCN etching. Thus, the sample did not contain any significant amount of secondary Cu selenides phases, even before the etching. This was confirmed by the observation that this absorber resulted in a reasonable device with 12.5% efficiency, without etching it. This device showed the typical characteristics of Cu-rich cells in terms of steep quantum efficiency response at long wavelengths [11]. The extrapolated activation energy of the V_{OC} (T) curve of the device made from the unetched absorber at 0 K showed values close to the band gap of Cu-rich CIS absorbers as presented in Fig. 6(a), indicating

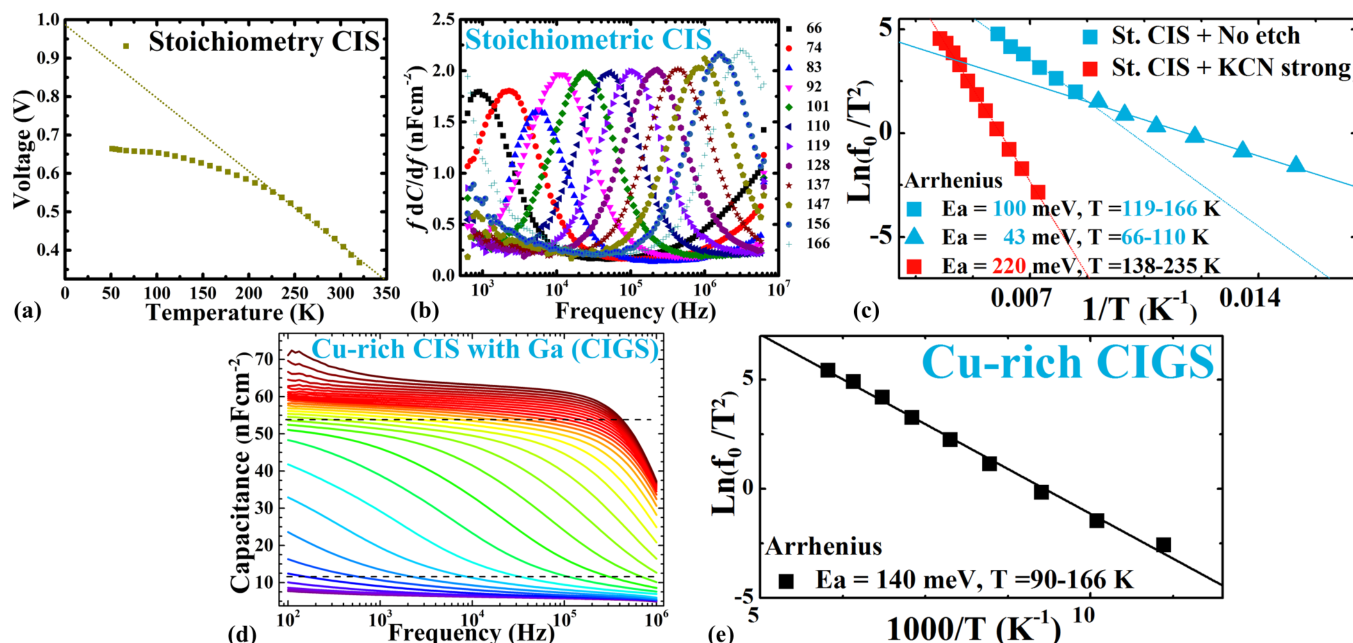

FIG. 6. (a) Temperature dependence V_{OC} and (b) capacitance derivative plot for unetched stoichiometric CIS. (c) Arrhenius plot for stoichiometric CIS absorber with (red) and without (blue) KCN strong etching with their corresponding activation energies of the main capacitance step and temperature ranges. (d) Admittance measurements with the temperature scale similar to the ones in Figs. 2 and 3. (e) Arrhenius plot for Cu-rich CIGS.

that the dominant recombination path is in the bulk of the absorber. Moreover, the ADM measurements performed on the stoichiometric absorber without etching showed narrow peaks for its capacitance derivative plot in Fig. 6(b) that resemble those of Cu-poor ones, indicating the presence of only one capacitance step. This capacitance step in the stoichiometric absorber is a double step with activation energies of 100 ± 10 and 50 ± 10 meV as presented in the Arrhenius plot of Fig. 6(c) (blue curves). The activation energies of this double step are close to those reported for high-performance Cu-poor CIS cells [44] and could be possibly related to the shallow acceptors: the second acceptor defect (A2 defect), in the donor-acceptor pair transition DA2 (activation energy of 100 ± 10 meV), and the first acceptor defect (A1 defect), in the donor-acceptor pair transition DA1 (activation energy of 50 ± 10 meV), observed by PL measurements [10]. There is no indication for the presence of the 200 ± 20 meV defect. This means that the origin of the 200 ± 20 meV defect lies not in stoichiometric phase itself, leaving the secondary phases and/or the etching process as a possible origin of this defect.

To confirm that and provide a final conclusion statement on this point, the same stoichiometric absorber was subjected to a strong KCN etching in a similar manner to the one performed on Cu-rich CIS absorbers before depositing an aluminum Schottky contact on the etched stoichiometric absorber [31,32]. ADM measurements were performed on that sample and the activation energy of the main capacitance step revealed values of 200 ± 20 meV as presented in Fig. 6(c) (red curve). The strong KCN etching process was also applied to Cu-poor CIS absorbers and the formation of the 200 ± 20 meV defect was confirmed [29]. Thus, the origin of the 200 ± 20 meV defect is the etching of the absorber, which is necessary in any Cu-rich absorber to remove Cu selenide phases before making it into a device.

Finally, we would like to mention that for Cu-rich $Cu(In, Ga)Se_2$ a similar effect of V_{OC} loss compared to Cu-poor cells is observed. This effect is partly alleviated by using a Ga PDT in the presence of high Se flux as reported [21]. We speculate that the same defect observed in Cu-rich $CuInSe_2$ is formed in Cu-rich $Cu(In, Ga)Se_2$ but is outside the detection limit of our ADM measurements. This defect is passivated in the presence of high Se flux that restores the lost V_{OC} [21] in a similar manner to Cu-rich $CuInSe_2$. ADM measurements were performed for a Cu-rich $Cu(In, Ga)Se_2$ absorber that was exposed to strong KCN etching as illustrated in Figs. 6(d) and 6(e). The 200 ± 20 meV defect is not visible and the activation energy of the main capacitance step indicated by the two short-dashed lines in Fig. 6(d) shows a value of 130 ± 10 meV [Fig. 6(e)] that changes with the addition of Ga corresponding to the third acceptor defect (A3 defect), in the donor-acceptor pair transition DA3, in an excellent agreement with the PL measurements reported [39].

III. EXPERIMENTAL SECTION

A. Synthesis of CI(G)S thin-film solar cells

Polycrystalline CIS and CIGS absorbers were fabricated on molybdenum coated soda-lime-glass. Both absorbers were fabricated using physical vapor deposition (PVD) in a Veeco molecular-beam epitaxy system. CIS was fabricated using a one-stage coevaporation process and $Cu(In, Ga)Se_2$ using a three-stage process. The Cu/III ratio was varied by controlling Cu and In fluxes. Absorbers grown under Cu-excess conditions were fabricated targeting an overall Cu/III ratio larger than 1, referred to in the text as "Cu rich." Absorbers fabricated with a Cu/III ratio of less than 1 are referred to in the text as "Cu poor." Elemental composition of the absorbers is determined through an Oxford instrument EDX with an acceleration voltage of 20 kV. This value represents the average composition of the absorber including Cu_xSe if present. After growth, the absorbers are subjected to a strong etching in a 10% aqueous solution of KCN for 5 min to remove copper selenide secondary phases [26,27]. For each absorber deposition run, four samples were produced. One absorber is reserved for different characterization techniques. One absorber is used as a bare absorber and etched, and a 3 μm Al layer is deposited using a Ferrotec electron-beam evaporation tool on top of the etched absorber to form a Schottky contact [31,32]. This type of device is referred to in the text as a "Schottky absorber." A thin CdS buffer layer was deposited on the remaining two etched absorbers through chemical-bath deposition. After that, an aluminum layer is again deposited on top of one of these two absorbers with buffer layers, referred to in the text as a "Schottky buffer." The remaining absorber with a CdS buffer layer is then further processed and finished by sputtering both a nominally undoped and a biased zinc oxide window layer [45] using an Aja Orion 8 sputtering tool. Finally, nickel-aluminum contacting grids were evaporated and this device is then referred to in the text as a "complete stack". The different absorber structures are illustrated in Fig. 1. A Se postdeposition treatment was developed in the context of this paper. Etched absorbers were returned to the PVD and exposed to an annealing step in the presence of Se-only with Se fluxes similar to those used for absorber growth the pressure of which is in the range of $4 - 5 \times 10^{-6}$ mbar for durations less than 8 min and at temperatures between 200 and 250 °C.

B. Characterization

The electrical parameters were extracted from the current-voltage (IV) measurements performed using a standard solar simulator, calibrated by a Si reference cell, with a Keithley IV-source-measure unit. In the setup used for temperature-dependent measurements, a cold mirror halogen lamp was used for illumination with an intensity of $100\,\mathrm{mW/cm^2}$. The activation energy of the dominant recombination channel and the IV characteristics as a function of temperature (IVT) were deduced from the IV characteristics [40] in a temperature range of 320–50 K using a CTI-cryogenic closed cycle helium cryostat. The illumination intensity at room temperature of the cold mirror halogen lamp was calibrated to the short-circuit current density (J_{SC}) determined from IV under standard test conditions. The CV as well as the temperature- and frequency-dependent admittance (admittance spectroscopy, ADM) measurements [28] were performed using the same IVT setup with a precision LCR meter.

CV measurements are performed to extract the apparent doping from the slope of the Mott-Schottky plot [Fig. 5(f)] at

a frequency of 100 KHz fitted at small forward bias (0.03–0.2 V) as indicated by the short-dotted lines in Fig. 5(f). This voltage range was chosen as the apparent doping at reverse bias could be influenced by either deep defects that could increase the apparent doping [40] or the doping level that could be depth dependent affected by Cd diffusion and decreasing the apparent doping at the interface [46]. ADM measurements are performed to study the electronic defect states in the semiconductor junction. The finite capture/emission time constants of such a defect level result in distinct steps in the admittance spectrum, which we have marked by the short-dashed lines in the experimental capacitance spectra presented in this paper (as in Fig. 2). The inflection frequency (f_t) of a capacitance step at a given temperature is determined by the defect response time, and the thermal activation energy of the defect can be obtained from the slope of an Arrhenius plot of the temperature-dependent inflection frequencies. Note that f_t is commonly scaled with a factor T^{-2} to account for implicit temperature dependences of the thermal velocity and effective density of states [28,47,48]. The presented approach to admittance spectroscopy requires that a given capacitance step is, in fact, caused by a defect level. This is often not the case for typical CIGS solar cells because transport barriers or secondary junctions in the device architecture, for example due to the buffer layer or a Schottky-type back contact, result in identical capacitance steps. When studying defects in CIGS by electronic measurements, it is thus mandatory to exclude effects that might be mistaken for defects by comparing the activation energy of the thermally activated series resistance and forward bias current as a function of temperature from one side to that extracted from ADM measurements on the other side. If one of the activation energies from series resistance or forward bias current as a function of temperature is in the same range as the activation energy from admittance measurements, then the admittance step is a transport barrier. Otherwise, if both activation energies (series resistance and forward bias current as a function of temperature) are less than those of admittance measurements, then this admittance step shall correspond to a defect [35,49]. PL measurements were performed using a continuous-wave solid-state laser diode with a wavelength of 660 nm for optical excitation. The generated PL is collected, guided into a monochromator, spectrally resolved, and detected by an InGaAs detector array. The samples are cooled down to 10 K in a liquid helium flow cryostat for measurements.

IV. CONCLUSION

A defect with an activation energy of 200 ± 20 meV was identified, that appears only in Cu-rich $CuInSe_2$ and not in Cu-poor absorbers. This defect is a Se-related acceptor defect present in the bulk near the surface of Cu-rich CIS absorbers. This defect is the responsible recombination center that shifts the dominant recombination path from the bulk to the interface, leading to a decrease in the V_{OC} and the deterioration of the efficiency of such cells. The strong KCN etching step mandatory to remove copper selenide secondary phases was shown to be the origin for the formation of this defect. The same etching step was applied on Cu-poor and stoichiometric CIS absorbers, resulting in the formation of the same 200 ± 20 meV defect. The defect can be passivated by any PDT containing Se including Se-only PDT as well as buffer layers with high enough chalcogen concentrations. The passivation of this defect leads to an improvement in the V_{OC}, FF, and efficiency of Cu-rich CIS solar cells.

ACKNOWLEDGMENTS

This paper has been funded by the Luxembourgish Fonds National de la Recherche in the framework of the Cu-rich CIS treated with potassium (K) (CURI-K), Surface passivation for thin film photovoltaics (SURPASS), and Materials for Sensing and Energy Harvesting (Massena) projects, which are gratefully acknowledged. Christian Andreas and Stephan Bücheler from EMPA are acknowledged for providing CdS buffer layer deposition.

[1] http://www.goech.at/files/The_7th_CS3_white_paper_12-March_small.pdf (2017).
[2] http://cigs-pv.net/wortpresse/wp-content/uploads/2015/12/CIGS-WhitePaper.pdf (2015).
[3] S. Siebentritt, Chalcopyrite compound semiconductors for thin film solar cells, Current Opinion Green Sustain. Chem. **4**, 1 (2017).
[4] http://www.solar-frontier.com/eng/news/2019/0117_press.html (2019).
[5] https://www.pv-magazine.com/2017/12/20/solar-frontier-hits-new-thin-film-cell-efficiency-record/ (2017).
[6] J. AbuShama, R. Noufi, S. Johnston, S. Ward, and X. Wu, Improved performance in $CuInSe_2$ and surface modified $CuGaSe_2$ solar cells, in *Proceedings of the IEEE Photovoltaics Specialists Conference and Exhibition* (IEEE PVSC, 2005), pp. 299–302.
[7] S. Siebentritt, L. Gütay, D. Regesch, Y. Aida, and V. Deprédurand, Why do we make $Cu(In, Ga)Se_2$ solar cells non-stoichiometric? Sol. Energy Mater. Sol. Cells **119**, 18 (2013).
[8] V. Depredurand, D. Tanaka, Y. Aida, M. Carlberg, N. Fevre, and S. Siebentritt, Current loss due to recombination in Cu-rich $CuInSe_2$ solar cells, J. Appl. Phys. **115**, 044503 (2014).
[9] F. Werner, D. Colombara, M. Melchiorre, N. Valle, B. El Adib, C. Spindler, and S. Siebentritt, Doping mechanism in pure $CuInSe_2$, J. Appl. Phys. **119**, 173103 (2016).
[10] S. Siebentritt, N. Rega, A. Zajogin, and M. Ch. Lux-Steiner, Do we really need another PL study of CuInSe2? Phys. Status Solidi C **1**, 2304 (2004).
[11] H. Elanzeery, F. Babbe, M. Melchiorre, A. Zelenina, and S. Siebentritt, Potassium fluoride ex-situ treatment on both Cu-rich and Cu-poor $CuInSe_2$ thin film solar cells, IEEE J. Photovoltaics **7**, 684 (2017).
[12] M. Turcu, O. Pakma, and U. Rau, Interdependence of absorber composition and recombination mechanism in $Cu(In, Ga)(Se, S)_2$ heterojunction solar cells, Appl. Phys. Lett. **80**, 2598 (2002).
[13] R. Mainz, H. Rodriguez-Alvarez, M. Klaus, D. Thomas, J. Lauche, A. Weber, M. D. Heinemann, S. Brunken, D. Greiner,

C. A. Kaufmann, T. Unold, H.-W. Schock, and C. Genzel, Sudden stress relaxation in compound semiconductor thin films triggered by secondary phase segregation, Phys. Rev. B **92**, 155310 (2015).

[14] R. Mainz, E. Simsek Sanli, H. Stange, D. Azulay, S. Brunken, D. Greiner, S. Hajaj, M. D. Heinemann, C. A. Kaufmann, M. Klaus, Q. M. Ramasse, H. Rodriguez-Alvarez, A. Weber, I. Balberg, O. Millo, P. A. van Aken, and D. Abou-Rasa, Annihilation of structural defects in chalcogenide absorber films for high-efficiency solar cells, Energy Environ. Sci. **9**, 1818 (2016).

[15] V. Depredurand, Y. Aida, J. Larsen, T. Eisenbarth, A. Majerus, and S. Siebentritt, Surface treatment of CIS solar cells grown under Cu-excess, in *Proceedings of the 37th IEEE Photovoltaic Specialists Conference* (IEEE PVSC, 2011), pp. 000337–000342.

[16] Y. Aida, V. Depredurand, J. K. Larsen, H. Arai, D. Tanaka, M. Kurihara, and S. Siebentritt, Cu-rich $CuInSe_2$ solar cells with a Cu-poor surface, Prog. Photovolt: Res. Appl. **23**, 754 (2015).

[17] D. Schmid, M. Ruckh, F. Grunwald, and H. W. Schock, Chalcopyrite/defect chalcopyrite heterojunctions on the basis of $CuInSe_2$, J. Appl. Phys. **73**, 2902 (1993).

[18] V. Deprédurand, T. Bertram, and S. Siebentritt, Influence of the Se environment on Cu-rich CIS devices, Physica B **439**, 101 (2014).

[19] T. Bertram, V. Deprédurand, and S. Siebentritt, In-Se surface treatment of Cu-rich grown $CuInSe_2$, in *Proceedings of the IEEE 40th Photovoltaic Specialist Conference* (IEEE PVSC, 2014), pp. 3633–3636.

[20] F. Babbe, H. Elanzeery, M. Melchiorre, A. Zelenina, and S. Siebentritt, Potassium fluoride post deposition treatment with etching step on both Cu rich and Cu poor $CuInSe_2$ thin film solar cells, Phys. Rev. Mater. **2**, 105405 (2018).

[21] L. Choubrac, T. Bertram, H. Elanzeery, and S. Siebentritt, $Cu(In, Ga)Se_2$ solar cells with improved current based on surface treated stoichiometric absorbers, Phys. Status Solidi A **214**, 1600482 (2017).

[22] C. Spindler, F. Babbe, M. H. Wolter, F. Ehré, K. Santhosh, P. Hilgert, F. Werner, and S. Siebentritt, Electronic defects in $Cu(In, Ga)Se_2$: Towards a comprehensive model (unpublished).

[23] F. Babbe, L. Choubrac, and S. Siebentritt, Quasi Fermi level splitting of Cu-rich and Cu-poor $Cu(In, Ga)Se_2$ absorber layers, Appl. Phys. Lett. **109**, 082105 (2016).

[24] F. Babbe, L. Choubrac, and S. Siebentritt, The optical diode ideality factor enables fast screening of semiconductors for solar cells, Solar RRL **2**, 1800248 (2018).

[25] T. Gödecke, T. Haalboom, and F. Ernst, Phase equilibria of Cu-In-Se I. Stable states and nonequilibrium states of the In_2Se_3-Cu_2Se subsystem, Z. Metallkd. **91**, 622 (2000).

[26] D. Regesch, L. Gütay, J. K. Larsen, V. Deprédurand, D. Tanaka, Y. Aida, and S. Siebentritt, Degradation and passivation of $CuInSe_2$, Appl. Phys. Lett. **101**, 112108 (2012).

[27] Y. Hashimoto, N. Kohara, T. Negami, M. Nishitani, and T. Wada, Surface characterization of chemically treated $Cu(In, Ga)Se_2$ thin films, Jpn. J. Appl. Phys. **35**, 4760 (1996).

[28] P. Blood and J. W. Orton, *The Electrical Characterization of Semiconductor: Majority Carriers and Electron States* (Academic, New York, 1992).

[29] D. Colombara, H. Elanzeery, N. Nicoara, D. Sharma, A. Koprek, M. Wolter, N. Valle, O. Bondarchuk, M. Melchiorre, F. Babbe, C. Spindler, O. Cojocaru-Miredin, D. Raabe, P. J. Dale, S. Sadewasser, and S. Siebentritt, Chemical instability of chalcogenide surfaces near phase boundaries (unpublished).

[30] T. Bertram, V. Depredurand, and S. Siebentritt, Electrical characterization of defects in Cu-rich grown $CuInSe_2$ solar cells, IEEE J. Photovoltaics **6**, 546 (2016).

[31] B. Theys, T. Klinkert, F. Mollica, E. Leite, F. Donsanti, M. Jubault, and D. Lincot, Revisiting Schottky barriers for CIGS solar cells: Electrical characterization of the $Al/Cu(InGa)Se_2$ contact, Phys. Status Solidi A **213**, 2425 (2016).

[32] E. Schlenker, V. Mertens, J. Parisi, R. Reineke-Koch, and M. Köntges, Schottky contact analysis of photovoltaic chalcopyrite thin film absorbers, Phys. Lett. A **362**, 229 (2007).

[33] A. Niemegeers and M. Burgelman, Effects of the Au/CdTe back contact on IV and CV characteristics of Au/CdTe/CdS/TCO solar cells, J. Appl. Phys. **81**, 2881 (1997).

[34] S. M. Sze and K. K. Ng, *Physics of Semiconductor Devices*, 3rd ed. (Wiley, New York, 2008).

[35] F. Werner, M. H. Wolter, S. Siebentritt, G. Sozzi, S. D. Napoli, R. Menozzi, P. Jackson, W. Witte, R. Carron, E. Avancini, T. Weiss, and S. Buecheler, Alkali treatments of $Cu(In, Ga)Se_2$ thin-film absorbers and their impact on transport barriers, Prog. Photovolt. Res. Appl. **26**, 911 (2018).

[36] See Supplemental Material at http://link.aps.org/supplemental/10.1103/PhysRevMaterials.3.055403 for the characteristics of the 200 ± 20 meV defect in Cu-rich $CuInSe_2$ thin-film solar cells.

[37] T. Bertram, Doping, defects and solar cell performance of Cu-rich grown $CuInSe_2$, Ph.D. thesis, University of Luxembourg, 2016, http://orbilu.uni.lu/handle/10993/28325.

[38] A. Chirila, P. Reinhard, F. Pianezzi, P. Bloesch, A. Uhl, C. Fella, L. Kranz, D. Keller, C. Gretener, H. Hagendorfer, D. Jaeger, R. Erni, S. Nishiwaki, S. Buecheler, and A. Tiwari, Potassium-induced surface modification of $Cu(In, Ga)Se_2$ thin films for high-efficiency solar cells, Nat. Mater. **12**, 1107 (2013).

[39] F. Babbe, H. Elanzeery, M. H. Wolter, K. Santhosh, and S. Siebentritt, Experimental verification of a third acceptor type defect in $CuInSe_2$ and $Cu(In, Ga)Se_2$ absorber layers (unpublished).

[40] D. Abou-Ras, T. Kirchartz, and U. Rau, *Advanced Characterization Techniques for Thin Film Solar Cells* (Wiley, New York, 2011).

[41] R. Scheer, Activation energy of heterojunction diode current in the limit of interface recombination, J. Appl. Phys. **105**, 104505 (2009).

[42] P. Zabierowski, U. Rau, and M. Igalsona, Classification of metastabilities in the electrical characteristics of $ZnO/CdS/Cu(In, Ga)Se_2$ solar cells, Thin Solid Films **387**, 147 (2001).

[43] M. Igalson, M. Bodegård, and L. Stolt, Reversible changes of the fill factor in the $ZnO/CdS/Cu(In, Ga)Se_2$ solar cells, Sol. Energy Mater. Sol. Cells **80**, 195 (2003).

[44] H. Elanzeery, F. Babbe, M. Melchiorre, F. Werner, and S. Siebentritt, High performance low bandgap thin film solar cells for tandem applications, Prog. Photovolt. Res. Appl. **26**, 437 (2018).

[45] M. Hála, H. Kato, M. Algasinger, Y. Inoue, G. Rey, F. Werner, C. Schubbert, T. Dalibor, and S. Siebentritt, Improved environmental stability of highly conductive nominally undoped ZnO

layers suitable for n-type windows in thin film solar cells, Sol. Energy Mater. Sol. Cells **161**, 232 (2017).

[46] F. Werner, T. Bertram, J. Mengozzi, and S. Siebentritt, What is the dopant concentration in polycrystalline thin-film $Cu(In, Ga)Se_2$? Thin Solid Films **633**, 222 (2017)

[47] T. Eisenbarth, T. Unold, R. Caballero, C. A. Kaufmann, and H.-W. Schock, Interpretation of admittance, capacitance-voltage, and current-voltage signatures in $Cu(In, Ga)Se_2$ thin film solar cells, J. Appl. Phys. **107**, 034509 (2010).

[48] F. Werner and S. Siebentritt, Buffer Layers, Defects, and the Capacitance Step in the Admittance Spectrum of a Thin-Film Solar Cell, Phys. Rev. Applied **9**, 054047 (2018).

[49] C. Schubbert, P. Eraerds, M. Richter, J. Parisi, I. Riedel, T. Dalibor, and J. Palm, A simulation study on the impact of band gap profile variations and secondary barriers on the temperature behavior, performance ratio, and energy yield of $Cu(In, Ga)(Se, S)_2$ solar cells, Phys. Status Solidi A **212**, 336 (2015).